# Three-Dimensional Simulations of the Implosion of Inertial Confinement Fusion Targets

R. P. J. Town and A. R. Bell

*Blackett Laboratory, Imperial College of Science, Technology and Medicine, London SW7 2BZ, United Kingdom*

(Received 28 March 1991)

The viability of inertial confinement fusion depends crucially on implosion symmetry. A spherical three-dimensional hydrocode called PLATO has been developed to model the growth in asymmetries during an implosion. Results are presented of the deceleration phase which show indistinguishable linear growth rates, but greater nonlinear growth of the Rayleigh-Taylor instability than is found in two-dimensional cylindrical simulations. The three-dimensional enhancement of the nonlinear growth is much smaller than that found by Sakagami and Nishihara.

PACS numbers: 52.35.Py, 52.65.+z

An important issue facing inertial confinement fusion (ICF) is implosion symmetry. A typical ICF target can be characterized as passing through three phases: acceleration, coasting, and deceleration [1]. Initially the shell is accelerated inwards and the Rayleigh-Taylor (RT) [2] instability grows on the outer ablation surface. When the shell reaches its maximum velocity it coasts inwards with no acceleration. Although not unstable, the large spherical convergence can amplify the distortion further. As the pressure inside the filler gas increases, the shell is decelerated and finally brought to rest. In this final stage the shell is again RT unstable, but this time on the inner fuel-shell interface.

In the acceleration phase 2D simulations [3–5] have shown a reduction in the RT linear growth rate to one-half of the classical value. This has been confirmed by experimental results [6]. Recent 3D results [7] in planar geometry have shown linear growth rates similar to 2D, but enhanced growth in the nonlinear regime. In the deceleration phase the RT instability is expected to behave classically. Simulations have been performed by Sakagami and Nishihara in cylindrical geometry in 2D [8] and recently using a Cartesian code in 3D [9]. Sakagami and Nishihara have found no difference in the 3D linear behavior compared to 2D. They find that the nonlinear regime obeys an $\eta g t^2$ law, with an $\eta$ up to 6 times the value of comparable 2D cylindrical simulations.

We report here on our simulations of the deceleration phase using PLATO. Our results are compared to similar 2D cylindrical and spherical simulations but we do not find the large increase in nonlinear growth as reported by Sakagami and Nishihara. PLATO is a 3D, spherical hydrodynamics code with a fixed Eulerian grid. The time-dependent equations of mass, momentum, and total energy are integrated numerically using the van Leer [10] algorithm as interpreted by Youngs [11]. The fluid equations are closed using an ideal ($\gamma = \frac{5}{3}$) equation of state. Currently thermal conduction, laser energy deposition, and $\alpha$-particle heating are not included. In order to accurately model implosions a fine resolution is needed. The large number of grid points needed to model a full sphere would require a large amount of memory and long run times. To reduce the memory requirement the computational grid was reduced from the full sphere by using the symmetry of Platonic solids.

At present we are employing the symmetry imposed on the target by the Rutherford Appleton Laboratory's twelve-beam Vulcan laser system. The point of intersection of the center of each laser beam with the target surface defines the symmetry of the target. These points form the vertices of twenty equilateral triangles on the surface. Since the triangles are equilateral the sides can be bisected and six smaller triangles formed from each equilateral one. Hence the smallest self-similar component is $\frac{1}{120}$ th of the sphere. This segment of the sphere is modeled in all our simulations. The exploitation of the symmetry imposed by the laser beams is valid when all the beams are balanced. Our modeling is consistent with the RT instability being seeded by the laser beam structures.

At the start of an ICF implosion a shock wave is launched into the stationary fuel. The shock wave is reflected at the origin and travels outward colliding with the incoming shell marking the beginning of the deceleration phase. To a good approximation we found that the radius of the inner surface ($R_1$) obeys $R_1 = R_{1,\mathrm{mc}} + 0.5g(t - t_{\mathrm{mc}})^2$, where $R_{1,\mathrm{mc}}$ is the inner surface radius at the time $t_{\mathrm{mc}}$ of maximum compression. When the central hot-spot region satisfies the conditions for fusion, it ignites and a burn wave propagates outwards. The deceleration phase ends at this time with the remainder of the shell rapidly expanding. In the absence of $\alpha$-particle heating the shell continues to obey the above equation for $R_1$. It is during this deceleration phase that the inner surface of the shell is RT unstable.

We started the simulations by modeling the coasting phase with a one-dimensional (1D) 60-$\mu$m-thick unperturbed shell of density 5.0 g/cm$^3$ at an initial radius of 130 $\mu$m coasting at a velocity of $1.5\times10^7$ cm/s into a stationary fuel of density 0.5 g/cm$^3$. The region outside the shell had a density of 0.5 g/cm$^3$ and the same initial inward velocity. A uniform pressure of $2.0\times10^{13}$ dyn/cm$^2$ was used in all regions. Because the acceleration is not modeled the initial shock is launched into the fuel with the shell already accelerated, which is not the case in real ICF implosions. When the reflected shock wave was al-

 

most incident on the inner surface of the shell, at 0.626 ns, the one-dimensional profiles were converted to 3D. The radial cells were uniform with a resolution of 0.5 $\mu$m. There were ten grid points in each of the $\theta$ and $\phi$ directions giving twenty cells per wavelength. Additional simulations performed with thirty cells per wavelength showed no substantial difference. In order to maximize the size of the cells the grid was uniformly spaced in $\phi$, but nonuniform in $\theta$. All boundaries were reflective, except the outer radial one, which was open. The 1D density profile was perturbed by imposing a variation of amplitude in the position of the inner surface. We assume that each laser beam generates the same angular pattern. The perturbation is thus the sum of the Legendre polynomials from all twelve beams. The lowest-order mode which can be imposed on a balanced twelve-beam system is the sixth-order Legendre polynomial summed over the laser beam poles.

The arrangement of the laser beam implies that the mass distribution $[\sigma(\theta,\phi)]$ can be expressed as the sum of all Legendre polynomials summed over the laser beams:

$$\sigma(\theta,\phi)=\sum_{n=0}^{\infty} a_n \sum_{b=1}^{12} P_n(\cos(\xi_b)) , \quad (1)$$

where the coefficient $a_n$ is the mass amplitude of the $n$th mode. In a way analogous to Fourier theory we can obtain the coefficient of the $k$th mode as follows. At selected times the mass distribution is obtained by integrating, from the center through the shell to the outer boundary, the product of the density and radius squared. This is multiplied by the $k$th Legendre polynomial and integrated over all angles. This gives us a measure of the RT growth, which we refer to as the mass mode amplitude. The evolution of the mass perturbation is a signature of the RT instability; in secular growth no such movement of mass would be noted. An alternative measure of the RT growth is to calculate the distance ($\Delta R_1$) between the tip of the spike ($R_{1,\min}$) and the head of the bubble ($R_{1,\max}$). The inner surface of the shell ($R_1$) is defined as the surface whose density is $1/e$ of the maximum density. Simulations were also performed using a constant-density definition for $\Delta R_1$; these showed almost identical growth rates.

First we model the linear regime by placing a small-amplitude ($\delta_0=0.005R_1$) perturbation on the target. With this perturbation we find linear growth with a growth rate of 5.41 $ns^{-1}$. For the simulation parameters the shell underwent an acceleration of $2.62\times10^{16}$ $cm\,s^{-2}$. Peak compression was achieved at 1.03 ns at a radius of $3.5\times10^{-3}$ cm. The Atwood number was approximately 0.84. This gives a classical planar growth rate of 6.15 $ns^{-1}$, implying a reduction to approximately 90% classical. Unlike the classical linear theory the inner-shell interface has a finite density gradient which may be responsible for the small reduction in the classical growth rate. Also, $\sqrt{k}$ changes during the implosion. 2D simulations

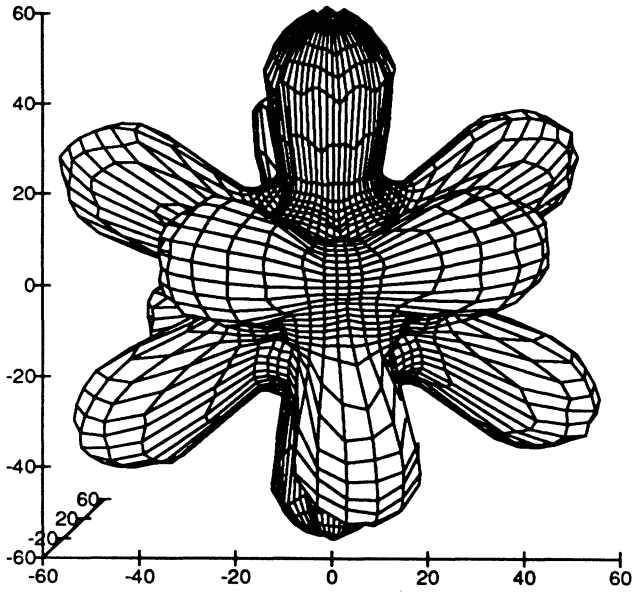


FIG. 1. The inner surface of the shell (defined as the surface of constant density equal to $1/e$ of the maximum density) at 1.226 ns. This shows the bubble-ridge arrangement.

with the same initial conditions were also performed in cylindrical and spherical geometry. The cylindrical case used $(r,\theta)$ geometry ignoring the $z$ direction. The spherical case used $(r,\theta)$ geometry allowing no dependence on the $\phi$ direction. Spherical geometry has a pole (the $z$ direction from which $\theta$ is measured) which is essentially a 3D feature. In 2D simulations we were able to use a finer resolution. The reduction from the classical growth rate in all the 2D simulations was identical to the reduction observed in 3D, doubtless because any 3D perturbation can be decomposed into a sum of spherical harmonics.

To assess the nonlinear behavior the initial amplitude of the perturbation was increased ($\delta_0=0.1R_1$) so that the linear regime saturated quickly. We have plotted in Fig. 1 the inner surface of the shell ($R_1$) near the end of the simulation at 1.226 ns. We see a single well-defined bubble rising up, surrounded by a series of interconnecting spikes falling to form ridges. We have termed this the "bubble-ridge" arrangement.

When we invert the initial perturbation ($\delta R\rightarrow -\delta R$), which physically means having strongly focused beams with little beam overlap, the shell distorts quite differently. Now thin spikes penetrate into the fuel which are surrounded by a valley of interconnecting bubbles. This we have termed the "valley-spike" arrangement. Although the initial perturbation is a pure inversion the simulation does not remain purely inverted. In particular, the bubble in the bubble-ridge arrangement breaks through the back of the shell, which was not observed in the valley-spike arrangement.

In Fig. 2 we plot the evolution of $\Delta R_1$ for both the nor-

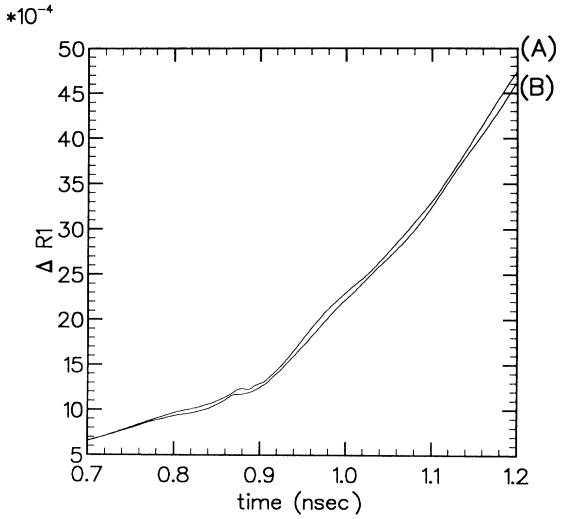


FIG. 2. The time evolution of the difference ($\Delta R_1$) between the head of the bubble and the tip of the spike for the bubble-ridge (curve *A*) and valley-spike (curve *B*) arrangements.

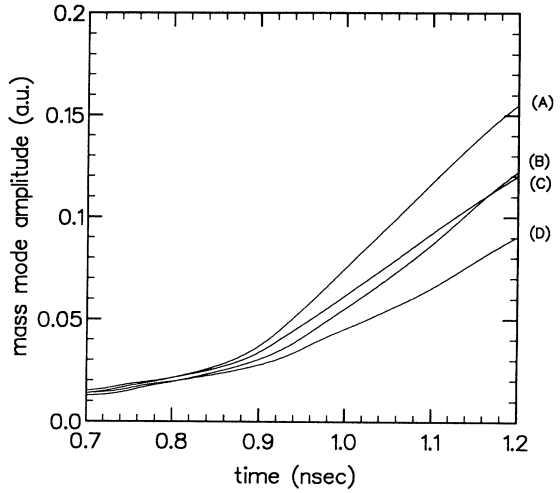


FIG. 3. The time evolution of the sixth-order mass mode amplitude for the bubble-ridge thin- (curve *A*) and thick-shell (curve *B*) and the valley-spike thin- (curve *C*) and thick-shell (curve *D*) simulations.

mal and inverted arrangements. We see that there appears to be no difference in the evolution and growth of each arrangement. We achieved a best fit by an $\eta g t^2$ law with a value of $\eta = 0.23$. We have compared this with corresponding simulations in 2D spherical and cylindrical geometries. The 2D spherical simulations were run with both a bubble at the pole and a spike at the pole; in both cases we find that $\eta$ has the slightly larger value of 0.25. However, in cylindrical geometry $\eta = 0.18$.

The evolution of the mass mode amplitude is quite different (Fig. 3) from that of $\Delta R_1$. Now the bubble-ridge arrangement has a higher growth rate than the valley-spike one. In both cases the mass mode amplitude evolves proportionally to $gt^2$. The mass is redistributed more quickly in the bubble-ridge arrangement, resulting in the earlier disruption of the shell. This conclusion is supported by 2D simulations. 2D spherical simulations with the bubble centered on the pole of the coordinate system show growth comparable with the 3D bubble-ridge arrangement. However, 2D cylindrical simulations show lower growth.

The differences between 2D and 3D and between the two 2D geometries can be explained by considering the nature of the bubble in the different geometries. In the bubble-ridge arrangement we have a truly 3D bubble surrounded by a ridge of interconnecting spikes. Similarly in the 2D spherical case, where a bubble is centered on the pole, the bubble is essentially 3D, surrounded by a ridge around the waist. In the 2D cylindrical case the bubble is in reality a valley running around the sphere. In the 3D case the bubble has a larger boundary to feed mass into the spike than in the 2D cylindrical case. Let us assume that the growth can be expressed as the product of the length of the boundary between the bubble and spike and the mass flux flowing across the boundary normalized to the area of the bubble. In 3D the bubble can be thought of as a hemisphere of radius $\lambda/4$ (where $\lambda$ is the wavelength of the perturbation). The perimeter of the bubble is $2\pi\lambda/4$ and the area of the hemisphere is $2\pi(\lambda/4)^2$. In 2D the bubble is a half cylinder of length $a$ and radius $\lambda/4$. The boundary between the bubble and spike is thus $2a$ and the area of the bubble is $a\pi\lambda/4$. In order to obtain $a$ in terms of $\lambda$ we compare the growth of bubbles with the same area; hence $a = \lambda/2$. The boundary in 2D is thus equal to $\lambda$. The boundary in 3D is $\pi/2$ larger than in 2D, allowing mass to pass from the bubble to the spike more easily in 3D, and hence giving a faster growth. Sakagami and Nishihara's results support this conclusion; faster growth occurs in spherical harmonics which maximize the boundary between bubble and spike.

Sakagami and Nishihara find a much larger difference between 2D and 3D. They find 0.2 in 2D, but $\eta = 0.8$–$1.1$ in 3D. The growth is characterized by them in terms of a mode amplitude calculated by integrating the mass density in the radial direction away from the center of the target. This can only be related to $gt^2$ (a distance) by scaling the amplitude by a dimensional quantity. There is considerable uncertainty in the required scaling factor which is further complicated by the change in density and size of the target as it compresses. We suspect that the explanation of their large $\eta$ lies in the choice of a scaling factor.

Youngs [12] has performed 2D and 3D simulations of the classical RT problem. He characterizes the amplitude in terms of a mixing width. In the earlier part of the nonlinear regime, before the small-scale turbulence has developed, he finds that 3D evolves 1.5 times faster than 2D. When small-scale turbulence has developed, then the

3D growth slows to that of 2D. Hence his 3D increase in the early phase of nonlinear growth is consistent with our results.

Let us now examine the differences between the two forms of 3D evolution by looking at the mass distribution $\sigma(\theta,\phi)$. The bubble-ridge arrangement always has less mass in its minimum radial line $[\sigma_{\min}(\theta,\phi)]$ and the rate at which it thins is always greater than in the valley-spike arrangement. Conversely, the valley-spike arrangement always has more mass in its maximum radial line $[\sigma_{\max}(\theta,\phi)]$ and the rate at which it thickens is always greater than in the bubble-ridge arrangement. The bubble-ridge arrangement is essentially better at bubble development, whereas the valley-spike arrangement is better at spike development. Shell thinning is therefore more rapid in the bubble-ridge arrangement. This shell thinning can cause the shell to break up, preventing further compression and allowing the fuel to escape. As the bubble increases in size, the mass of the shell at the bubble head is reduced, leading to a higher acceleration relative to the rest of the shell. The bubble then sheds mass more quickly. This suggests that thinner shells would have a more rapid evolution of the bubble. The valley-spike geometry has less well developed bubbles so the effect of the shell thinning would not be as important. Curve *A* of Fig. 3 shows the growth of the bubble-ridge arrangement with a shell of two-thirds the thickness, but with the same mass, showing higher growth than the thicker shell.

In conclusion, we have reported 3D simulations of the deceleration phase of an ICF target. We have obtained linear RT growth rates which are 90% of the classical value. These have been found to be identical to similar 2D cylindrical and spherical results. In the nonlinear regime we have found a faster mode evolution in 3D simulations than in 2D cylindrical geometry. This has been attributed to the greater bubble-spike boundary in 3D. We have observed two possible geometries in which the RT instability can grow in 3D: the bubble-ridge and valley-spike arrangements. The mass mode evolution of the bubble-ridge geometry is faster. Shell integrity is maintained for longer if the shell is driven more strongly immediately under the beams rather than at the intersections of the beams. We do not find the much greater nonlinear growth in 3D found by Sakagami and Nishihara.

We would like to thank Dr. D. L. Youngs of A. W. E. Aldermaston and Professor M. G. Haines of Imperial College for their useful discussions and comments. This work was financially supported by the Science and Engineering Research Council.

[1] D. L. Book and S. E. Bodner, Phys. Fluids **30**, 367 (1987).
[2] Lord Rayleigh, *Theory of Sound* (Dover, New York, 1945), 2nd ed.; G. I. Taylor, Proc. Roy. Soc. London A **201**, 192 (1950).
[3] M. Tabak, D. H. Munro, and J. D. Lindl, Phys. Fluids B **2**, 1007 (1990).
[4] J. H. Gardner, S. E. Bodner, and J. P. Dahlburg, Phys. Fluids B **3**, 1070 (1991).
[5] C. P. Verdon *et al.*, Phys. Fluids **25**, 1653 (1982).
[6] M. Desselberger, O. Willi, M. Savage, and M. J. Lamb, Phys. Rev. Lett. **65**, 2997 (1990).
[7] J. P. Dahlburg and J. H. Gardner, Phys. Rev. A **41**, 5695 (1990).
[8] H. Sakagami and K. Nishihara, Phys. Fluids B **2**, 2715 (1990).
[9] H. Sakagami and K. Nishihara, Phys. Rev. Lett. **65**, 432 (1990).
[10] B. van Leer, J. Comput. Phys. **23**, 276 (1977).
[11] D. L. Youngs, *Numerical Methods for Fluid Dynamics* (Academic, New York, 1982).
[12] D. L. Youngs (to be published).